ELSEVIER

Journal of Fluids and Structures 19 (2004) 575–590

JOURNAL OF FLUIDS AND STRUCTURES

www.elsevier.nl/locate/jnlabr/yjfls

Reduced-order modelling of limit-cycle oscillation for aeroelastic systems ☆

P.S. Beran[a,*], D.J. Lucia[b], C.L. Pettit[a]

[a] *Multidisciplinary Technologies Center, Air Vehicles Directorate, AFRL/VASD, Building 146, 2210 Eighth Street, WPAFB, OH 45433, USA*

[b] *Structures Division, Air Vehicles Directorate, AFRL/VAS, Building 45, 2130 Eighth Street, WPAFB, OH 45433, USA*

Received 23 September 2003; accepted 19 January 2004

Abstract

Limit-cycle oscillations (LCOs) of a nonlinear panel in supersonic flow are computed using a reduced-order aeroelastic model. Panel dynamics are governed by the large-deflection, nonlinear, von Kármán equation as expressed in low-order form through a Galerkin approximation. The aerodynamics are described by the Euler equations, which are reduced in order using proper orthogonal decomposition. The coupled system of equations is implicitly time integrated with second-order temporal accuracy to predict LCO amplitude, and linearly analyzed to predict LCO onset. The fluid is synchronized with the structure in time through subiteration, using only 18 dof to describe the aeroelastic system. The Jacobian employed in the fully implicit analysis is of equivalently low rank, enabling rapid analysis. Using the reduced-order model, LCO onset is predicted directly at a computational cost of approximately 400 time steps with a high accuracy verified by full-order analysis.

Published by Elsevier Ltd.

1. Introduction

Over the last several years, Karhunen–Loève (K–L) analysis, or proper orthogonal decomposition (POD), has been used to accelerate greatly the time integration of aeroelastic configurations by reducing system order (Romanowski, 1996; Hall et al., 2000; Thomas et al., 2001). While the application of POD to aeroelastic systems has been primarily limited to linearized aerodynamic analysis, these studies show the tremendous potential of POD-based reduced-order models (ROMs) for the economical stability analysis of aeroelastic configurations. POD-based ROMs have also been applied in different forms to problems in many disciplines. Noteworthy achievements with POD-based ROMs include: the development of control models for unsteady flow (Park and Lee, 1998; Rediniotis et al., 1999), airfoil shape optimization (LeGresley and Alonso, 2000, 2001), Euler analysis of unsteady flows driven by structural vibration (Pettit and Beran, 2000), and the study of nonlinear oscillations in flexible panels (Mortara and Beran, 2000). A review of relevant work is given by Beran and Silva, 2001.

The determination of aeroelastic behavior in the transonic regime is an especially demanding problem owing to the capture of essential nonlinearities in the aerodynamics. System nonlinearities, which may include structural nonlinearities, also play a key role in the aeroelastic phenomenon of limit-cycle oscillation (LCO) (Dobbs et al., 1985;

☆ The views expressed in this article are those of the authors and do not reflect the official policy or position of the United States Air Force, the Department of Defense, or the US Government.

*Corresponding author.

E-mail address: philip.beran@wpafb.af.mil (P.S. Beran).

0889-9746/$ - see front matter Published by Elsevier Ltd.
doi:10.1016/j.jfluidstructs.2004.04.002

Cunningham, 1998; Gordnier and Melville, 1998; Beran et al., 1999). To capture properly the effects of aerodynamic nonlinearities on aeroelastic behavior, time-integration methods based on the transonic small-disturbance, Euler and Navier–Stokes equations have been developed. These methods can provide accurate approximations of system behavior, but generally require very large computation times owing to the time-accurate nature of the calculations and the large integration times required to establish flow stability properties. Direct methods formulated from Hopf bifurcation theory have been developed to compute flutter and LCO onset speeds of aeroelastic systems without time integration [Beran and Morton (1997); Beran (1998); Morton and Beran (1999); Beran (1999)], but become computationally expensive when system order becomes large.

Recent work has been carried out to apply POD to the Euler equations in an effort to capture aerodynamic nonlinearities in a reduced-order aeroelastic model. A low-order POD representation of the discrete, two-dimensional Euler equations [Pettit and Beran (2000)] was coupled with the von Kármán equation to simulate the dynamics of flow over a flexible panel [Beran and Pettit (2001)]. For supersonic flows that were essentially linear (Mach 1.2), LCOs were accurately computed with the POD model using time steps of moderate size. Following this success, a new approach was taken, involving domain decomposition, that allowed LCO to be accurately simulated in the transonic regime (Lucia et al., 2002). In that study, full-order and ROMs of a small flow region containing a moving shock were decomposed from the larger flow domain. Both approaches enabled a physically consistent treatment of the aerodynamic nonlinearity.

Like the previous work (Beran and Pettit, 2001), a single-domain approach is pursued in this investigation for flow conditions that are dominantly linear. However, the methodology is substantially altered to improve the temporal coupling between the aerodynamic and structural dynamic equations, thereby greatly increasing the allowable time step and decreasing the computational effort necessary to achieve LCO. Furthermore, a modal representation of the structure is employed, which permits a more efficient formulation of the reduced order aeroelastic system, further increasing computational efficiency. The modal representation also permits judicious application of structural damping to temper the spurious behavior of some eigenvalues of the low-order aeroelastic system that apparently arises from the form of data sampling used to construct the ROM. With very small amounts of damping, a direct method is used to predict the onset of LCO at a Hopf bifurcation point at least two orders of magnitude faster than with the full order model.

2. Formulation

We first summarize the governing equations for the structure and fluid, including boundary and initial conditions. The process by which these equations are discretized and then numerically integrated is described. The combined set of discrete equations will be referred to as the "full" system. Next described is the procedure by which the aerodynamic equations are projected onto a sub-space defined by the POD and then coupled to the structural dynamics equations. Attention will also be given to the computation of bifurcation points of the reduced-order aeroelastic system and the discretization of the physical domain.

2.1. Structural dynamics equations

Two-dimensional flow over a semi-infinite, pinned panel of length L is considered. Panel dynamics are computed with von Kármán's large-deflection plate equation, which is placed in nondimensional form using aerodynamic scales L and freestream velocity, u_∞ (Selvam and Morton, 1998) $(0<x<1)$

$$\frac{\mu}{\lambda}\frac{\partial^4 w}{\partial x^4} - N_x\frac{\partial^2 w}{\partial x^2} + \frac{\partial^2 w}{\partial t^2} = \mu\left(\frac{1}{\gamma M_\infty^2} - p\right), \tag{1}$$

$$N_x \equiv \frac{6\mu}{\lambda}\left(\frac{h}{L}\right)^{-2}(1-\nu^2)\int_0^1 \left(\frac{\partial w}{\partial x}\right)^2 \mathrm{d}x, \tag{2}$$

where h is the panel thickness, ρ_∞ is the freestream density, p is the pressure, scaled by $\rho_\infty u_\infty^2$, γ is the ratio of specific heats (1.4), M_∞ is the freestream Mach number, ν is Poisson's ratio (0.3), μ is the mass ratio $\rho_\infty L/\rho_s h$, ρ_s is the structural density, λ is a dynamic pressure parameter $(\rho_\infty u_\infty^2 L^3/D)$, D is the plate stiffness $(E_s h^3/12(1-\nu^2))$, and E_s is Young's modulus.

The nonlinear, in-plane load, (2), serves to limit panel deflections $w(x,t)$ induced by fluid–structure interaction. Here, the load is assumed to be distributed uniformally over the panel, as originally specified by Dowell (1966). Eq. (1) is comparable to the form Dowell studied, although the dimensional panel thickness, w_d, and dimensional time, t_d, are

scaled by h and $(\rho_s h L^4)^{1/2}$, respectively. Two pinned boundary conditions are enforced at the panel's endpoints: $w = 0$ and $\partial^2 w/\partial x^2 = 0$.

A modal solution for the deflection $w(x, t)$ is assumed

$$w(x,t) = \sum_{i=1}^{I_m} a_i(t)\sin(i\pi x), \tag{3}$$

where I_m is the number of structural modes retained, and the modal amplitudes a_i vary in time and are collocated in the array a. In the manner pursued by Dowell, 1966, the Galerkin method is used to obtain a low-order set of ordinary-differential equations describing the behavior of a_i. First, (3) is substituted into (1). The resulting expression is then integrated, following pre-multiplication by $\sin(i\pi x)$, to yield ($i = 1, \ldots, I_m$)

$$\frac{1}{2}\ddot{a}_i + \frac{\mu(i\pi)^4}{2\lambda}a_i + \frac{6\mu}{\lambda}\left(\frac{h}{L}\right)^{-2}(1-\nu^2)\alpha\frac{(i\pi)^2}{2}a_i = \mu P_i, \tag{4}$$

where $\alpha \equiv \sum_r a_r^2 (r\pi)^2/2$ and

$$P_i \equiv \int_0^1 \left(\frac{1}{\gamma M_\infty^2} - p\right)\sin(i\pi x)\,\mathrm{d}x. \tag{5}$$

The projected pressure components, P_i, are integrated from the aerodynamic solution with the midpoint rule, using flowfield pressures obtained at grid points on the panel surface. The aerodynamic equations, their discretization, and their solution are discussed in later sections. The form of (4) is equivalent to that arrived at by Dowell, although two differences should be noted. First, the different form of scaling described above alters equation coefficients, and, second, an expression relating p to the state of the panel is not assumed.

The structural dynamics equation (4) is placed in first-order form by introducing a mode speed array, b, such that $\dot{a}_i = b_i$,

$$\dot{b}_i = -\left[\frac{\mu(i\pi)^4}{\lambda} + \frac{6\mu}{\lambda}\left(\frac{Li\pi}{h}\right)^2(1-\nu^2)\alpha\right]a_i + 2\mu P_i - \zeta_i b_i, \tag{6}$$

where ζ_i is a coefficient for damping of the ith structural mode. Structural damping is used in the reduced order analysis, as will be described. The mode speeds and amplitudes are collocated into a structural solution array over all nodes, $Y_s = [b, a]^{\mathrm{T}}$, leading to a general form of the structural equation

$$\dot{Y}_s = R_s(Y_s, P; \mu, \lambda, h/L). \tag{7}$$

2.2. Fluid equations and boundary conditions

The flow above the pinned panel is modelled with the Euler equations, cast in nondimensional form for a general curvilinear coordinate system, (ξ, η). The panel is assumed to lie in a flat plane, extending towards $x = \pm\infty$, with the y-coordinate extending normal to the plane and the ξ and η, coordinates aligned with the x and y, coordinates. The fluid equations are expressed as

$$\frac{\partial \hat{U}}{\partial t} + \frac{\partial \hat{E}(U)}{\partial \xi} + \frac{\partial \hat{F}(U)}{\partial \eta} = 0, \tag{8}$$

where $\hat{U} \equiv U/(\xi_x\eta_y - \xi_y\eta_x)$, U is the array of conserved variables, and $\hat{E}$ and $\hat{F}$ are appropriate flux arrays. The aerodynamic equations are discretized in space to second-order accuracy with an upwind total variation diminishing (TVD) scheme previously applied to unsteady aerodynamic and aeroelastic problems (Pettit and Beran, 2000; Beran and Morton, 1997). Following discretization, the aerodynamic equations take the form

$$\dot{Y}_f = R_f(Y_f, Y_s; M_\infty), \tag{9}$$

where R_f is a collocation of the discrete fluid equations, and Y_f is the fluid-state array.

To simplify the construction of the ROM of the fluid, a transpiration boundary condition is applied at $y = 0$ to model the effects of a moving boundary without grid deformation (Sankar et al., 1986; Pettit and Beran, 2000). This transfer of boundary conditions is identical to that employed in small-disturbance theory, and assumes the regularity of the computed solution and the smallness of the deformation: $w(x) \ll 1$. Such small deformations are consistent with the deflections associated with panel response, especially near critical points of LCO onset. We also compare the panel-response solutions obtained in this study to those previously reported by Gordnier and Visbal, 2000 who used a

geometrically exact boundary condition at the panel surface. Along the three remaining boundaries of the computational domain, freestream conditions are specified.

2.3. Time integration of the coupled full-order equations

The systems of discretized fluid dynamic equations and modal structural equations are combined into a single time-dependent system representative of the complete interaction between structure and inviscid flow

$$\dot{Y} = R(Y; M_\infty, \mu, \lambda, h/L), \tag{10}$$

where $Y \equiv [Y_f, Y_s]^{\mathrm{T}}$ and $R \equiv [R_f, R_s]^{\mathrm{T}}$. We will refer to (10) as the "full-order" system, in that all aerodynamic dof are retained. A reduced-order system is derived below for which only significant dof are retained.

Following Beran (2001), time integration of (10) proceeds in two steps, assuming an $\mathcal{O}(\Delta_t)$ lag in the synchronization of fluid and structure, where Δ_t is the time step. First, the structural variables are updated from time level n to $n+1$ using a Crank–Nicolson procedure to be described below (but limited here to only structural variables). During this step, the pressures known at grid points on the panel surface are considered frozen. In the second step, the aerodynamic variables are explicitly updated, $Y_f^{n+1} = Y_f^n + \Delta_t R_f^n$, using only structural variables defined at time level n.

2.4. Grid generation and time step

The flow is simulated over a physical domain of length D_L, centered about $x = 0$, and height D_H. The domain is discretized using I nodes in the streamwise direction and J nodes normal to the panel. Indices i ($1 \leqslant i \leqslant I$) and j ($1 \leqslant j \leqslant J$) are used to denote grid points at which variables are evaluated. Grid points are clustered in the direction normal to the panel at the panel surface, with minimum spacing denoted by Δ_{wall}. The spacing of grid points is specified to grow geometrically with j from the panel boundary. In the streamwise direction, the node spacing is chosen to be uniform over the deforming panel segment (coincident with the structural grid), while growing geometrically upstream of the leading edge (positioned at $i = I_{LE}$) and downstream of the trailing edge (positioned at $i = I_{TE}$). Calculations are carried out with a baseline grid given by the following: $I = 141$, $J = 116$, $D_L = 50$, $D_H = 25$, $I_{LE} = 45$, $I_{TE} = 97$, and $\Delta_{\mathrm{wall}} = 0.0125$.

The full-order equations are time integrated with a time step of 0.005. A previous investigation (Beran and Pettit, 2001) found that the computed solutions of the coupled full-order equations were not sensitive to changes in the values of the grid parameters and the time step for the range of problems studied in this investigation.

2.5. POD

POD is a linear method for establishing an optimal basis, or modal decomposition, of an ensemble of continuous or discrete functions. Detailed derivations of the POD and its properties are available elsewhere (Holmes et al., 1996; Newman, 1996) and not repeated herein. In our discussion of POD, M basis vectors are used to represent deviations of $X(t)$, an N-dimensional vector, from a base solution, X_0. These are written as $\{e^1, e^2, \ldots, e^M\}$, and are referred to here as "modes." The modes are orthonormal

$$e^{i\mathrm{T}} e^j = \begin{cases} 1 & \text{if } i = j, \\ 0 & \text{otherwise} \end{cases} \tag{11}$$

and computed in a manner to be described shortly. The modal decomposition of $X(t)$ using M modes is given by

$$X(t) \approx X_0 + \sum_{i=1}^{M} \hat{X}_i e^i = X_0 + \Phi \hat{X}(t), \tag{12}$$

where Φ is an $N \times M$ matrix containing the ordered set of modes, $\Phi = [e^1, e^2, \ldots, e^M]$ and $\hat{X}$ is an M-dimensional vector of modal amplitudes, $\hat{X} = [\hat{X}_1, \hat{X}_2, \ldots, \hat{X}_M]$. For the method to be advantageous, $M \ll N$ is required.

The POD modes are constructed, or trained, by first computing samples, or snapshots, of system behavior (solutions at different instants in time for dynamic problems, or equilibrium solutions at different parameter values for static problems) and storing these samples in a snapshot matrix, $\mathscr{S}$. For now, we assume that M samples of solution deviation from the base state, X_0, are collected and column-wise collocated into the $N \times M$ snapshot matrix: $\mathscr{S} = [X_1 - X_0, X_2 - X_0, \ldots, X_M - X_0]$. The well-known K–L POD basis minimizes the error in approximating a member of this class with fewer than M basis vectors. This property of optimal convergence associated with the K–L basis is established in many works (Holmes et al., 1996; Newman, 1996; Hall et al., 2000). The K–L basis can be readily computed by relating a mode matrix Φ to the snapshot matrix through a transformation matrix V, $\Phi = \mathscr{S} V$, that

maximizes the projection of the snapshot matrix onto the POD basis. This leads to the eigenproblem

$$\mathscr{S}^{\mathrm{T}}\mathscr{S}V = V\Lambda \tag{13}$$

for eigenvectors V and eigenvalues Λ. The eigenvalues are nonnegative, since $\mathscr{S}^{\mathrm{T}}\mathscr{S}$ is symmetric and positive semi-definite. Provided that the eigenvectors V are scaled to be orthonormal, $V^{\mathrm{T}}V = I$ (I is the identity matrix), the transformation formula $\Phi = \mathscr{S}V$ yields $\Phi^{\mathrm{T}}\Phi = \Lambda$. Multiplying each e^i by $\sqrt{\Lambda_i}$ yields an orthonormal set of modes, $\Phi^{\mathrm{T}}\Phi = I$, as originally specified. The K–L basis for a subspace of dimension $M_r < M$ is obtained by retaining the modes associated with the M_r largest eigenvalues computed in (13). These retained modes are placed in the array Φ_r, such that $\Phi_r = \mathscr{S}V_r$.

2.6. POD applied to the fluid equations

The ROM of the full fluid system is obtained by substituting $Y_f = Y_0 + \Phi_r\hat{Y}_f$ into (9) and projecting the result onto the K–L basis, a process we call subspace projection. The reduced-order system takes the first-order form (where Y_0 represents uniform flow)

$$\dot{\hat{Y}}_f = \Phi_r^{\mathrm{T}} R_f(Y_0 + \Phi_r\hat{Y}_f, Y_s; M_\infty) \equiv \hat{R}_f. \tag{14}$$

In the POD analysis described above, the full-system state vector is assembled with the set of modes Φ_r. For systems with multiple dof per grid point, we have experienced algorithmic difficulties when linking field variables within individual modes. Instead, we represent each field variable separately by a set of modes. The process of computing modes and POD eigenvalues for equation sets with arbitrary numbers of variables is generalized by expanding the snapshot data into a larger matrix $\hat{\mathscr{S}}$, where each column is filled with sampled data only over a variable's index range. In this form, $\hat{\mathscr{S}}^{\mathrm{T}}\hat{\mathscr{S}}$ is a diagonal matrix of blocks, each of which is analyzed for POD eigenvectors and eigenvalues. For the Euler equations, computed modes may be associated with density or total energy, for example. Currently, we use the magnitude of POD eigenvalues to restrict the number of retained modes, regardless of the association between field variables and retained modes.

2.7. ROM construction and equation coupling

Application of a POD-based ROM to aeroelastic analysis involves two steps. First, the ROM is constructed using samples of full-system behavior taken for a set of input parameter values that are representative of relevant cases. These samples are computed by time-integration of the full-system equations, as described above, and then applied to the calculation of Φ_r. Details concerning the generation of samples is reserved for the Results section, including number of samples, duration of sampled behavior, and number of retained modes.

Later in this paper, we examine the application of ROMs to aeroelastic analysis at values of λ in the neighborhood of that used in the sampling process. We assess the λ-range of validity of these models in terms of ability to predict time-accurate estimates of $Y(t)$ and examine the extent to which time steps in the ROM analysis can exceed those limited by numerical stability in the full-system analysis.

The systems of reduced-order aerodynamic equations and modal structural equations are now combined into a low-order, aeroelastic system for the POD and structural modes

$$\dot{\hat{Y}} = \hat{R}(\hat{Y}; M_\infty, \mu, \lambda, h/L), \tag{15}$$

$$\hat{Y} \equiv [\hat{Y}_f, Y_s]^{\mathrm{T}}, \quad \hat{R} \equiv [\hat{R}_f, R_s]^{\mathrm{T}}.$$

2.8. Bifurcation analysis

With reduced-order modelling, critical parameter values at which the panel loses stability to time-periodic disturbances can be directly determined. This approach has been studied previously for a simple, nonlinear system involving convection, diffusion and reaction that exhibits Hopf bifurcation (Beran et al., 1999). Stability exchange in the form of a Hopf bifurcation occurs when a complex pair of eigenvalues of the Jacobian of the reduced-order aeroelastic system, $\hat{J}$, has a vanishing real part, while other real components of the eigenvalues of $\hat{J}$ are negative. The reduced-order Jacobian is computed numerically with central-difference approximations from the form

$$\hat{J} = \begin{bmatrix} \dfrac{\partial \hat{R}_f}{\partial \hat{Y}_f} & \dfrac{\partial \hat{R}_f}{\partial Y_s} \\ \dfrac{\partial R_s}{\partial \hat{Y}_f} & \dfrac{\partial R_s}{\partial Y_s} \end{bmatrix} \tag{16}$$

and is of a small rank equal to the number of retained fluid modes and structural dof. Choosing λ as a parameter to be varied, we define β such that $\beta(\lambda)$ is the real part of the eigenvalue of $\hat{J}(\lambda)$ with largest real part. A two-step procedure is conducted to search for points of stability exchange satisfying $\beta = 0$. First, a coarse sweep in λ is carried out, starting from a known, stable condition, and increasing λ until a positive value of β is computed. At each point in the sweep, a new Jacobian is numerically constructed from the reduced-order system. When a change in stability is detected, an iterative process of bi-section is followed, including $\hat{J}$ updates, that rapidly establishes the location of the bifurcation point to 5 significant digits in λ.

2.9. Time integration of the aeroelastic system

The aeroelastic system $\dot{\hat{Y}} = \hat{R}$ is integrated in time with the two-time level, second-order accurate, Crank–Nicolson method:

$$\frac{\hat{Y}^{n+1} - \hat{Y}^n}{\Delta_t} = \frac{1}{2}(\hat{R}^{n+1} + \hat{R}^n), \tag{17}$$

$$\mathscr{R} \equiv \hat{Y}^{n+1} - \frac{\Delta_t}{2}\hat{R}^{n+1} - \hat{Y}^n - \frac{\Delta_t}{2}\hat{R}^n = 0. \tag{18}$$

At each time level, $\mathscr{Y} \equiv \hat{Y}^{n+1}$ is computed from (18) using a chord technique with a time-frozen Jacobian

$$\left(I - \frac{\Delta_t}{2}\hat{J}_o\right)(\mathscr{Y}^{k+1} - \mathscr{Y}^k) = -\mathscr{R}(\mathscr{Y}^k), \tag{19}$$

where k is a subiteration index and $\hat{J}_o$ is the Jacobian of the reduced order aeroelastic system, evaluated for a condition of uniform flow and $Y_s = 0$. A suitable number of subiterations are computed at each time step to obtain a good approximation to $\hat{Y}^{n+1}$; typically, one to two subiterations are generally sufficient to drive $\mathscr{R}$ to near machine zero. We observe that for the cases examined herein, peak panel deflection is no more than 2% of panel length, thus allowing the chord method to be rapidly convergent. Prior to subiteration, $\mathscr{Y}$ is predicted from the explicit formula

$$\mathscr{Y} = \hat{Y}^n + \Delta_t \hat{R}^n. \tag{20}$$

Owing to the low order of the implicit system, the computational effort required to obtain $\mathscr{Y}$ is dominated by the expense of evaluating R.

The initial condition is that of uniform flow about an un-deflected panel with a perturbation to the first mode: $a_s(1) = \delta_{\text{pert}}$. Generally, $\delta_{\text{pert}} = 0.0001$ is specified.

3. Results

Steady state and dynamic aeroelastic states are computed for the aeroelastic configuration described above. Freestream Mach number, M_∞, and the dynamic pressure parameter, λ, are treated as free parameters, while μ, ν, and h/L, are specified to be 0.1, 0.3, and 0.002, respectively. This set of parameter values is selected to facilitate comparison with previous analysis, as will be described shortly. Using full-order analysis, results are computed at Mach 0.9 and 1.2, where steady state and LCO behavior is observed, respectively. Reduced order modelling is applied to the numerical prediction of the pitchfork bifurcation of steady state solutions at Mach 0.9 and the Hopf bifurcation of LCO solutions at Mach 1.2. Also, at Mach 1.2, LCO states of the reduced-order aeroelastic system are computed and compared to those found with the more computationally expensive full-order analysis.

3.1. Full-order analysis

Prior to discussion of results obtained with the reduced-order aeroelastic model, we present static and dynamic aeroelastic solutions of the full-order equations and assess their sensitivity to the number of structural modes. Solutions are compared to those reported by Gordnier and Visbal, 2000 for a variety of Mach numbers and dynamic pressures.

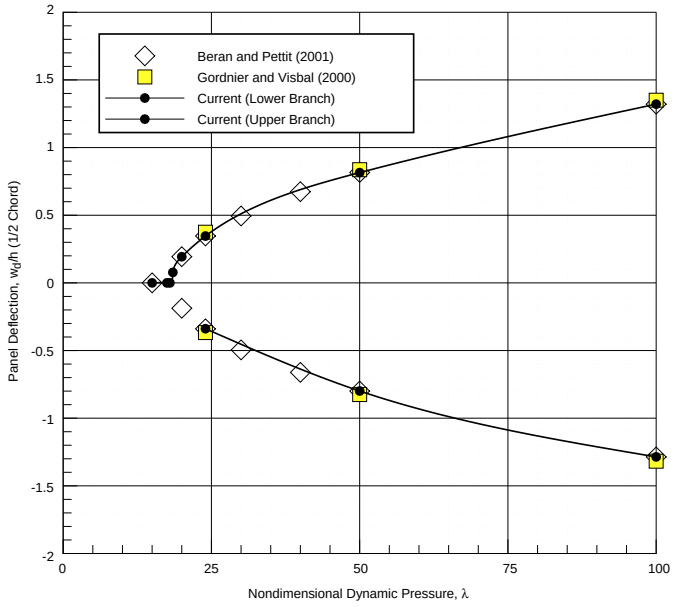

Fig. 1. Comparison of static deflections at the panel mid-chord for Mach 0.90 and selected dynamic pressures ($I_m = 4$).

Steady solutions are compared for Mach 0.9 and LCO solutions are compared for Mach 1.2. In all cases, agreement with published data is very good, providing confidence in the full-order model that has been constructed for this work.

At Mach 0.9, two branches of steady solutions bifurcate symmetrically from the trivial solution of a flat panel at a critical value of λ. At values of λ above critical, the trivial solution is unstable, and the selection of steady state solutions is determined from initial conditions. Computed results are shown in Fig. 1 in terms of thickness-normalized panel deflection at the mid-chord panel position ($x = 0$) where deflection is observed to be largest in magnitude. Data is reported for the case of 4 structural modes. Solutions are not found to be sensitive to I_m; mid-chord deflections (w_d/h on top branch) of 1.3211 ($I_m = 4$), 1.3210 ($I_m = 3$), and 1.2977 ($I_m = 2$) are computed. Also shown in Fig. 1 are data points reported by Gordnier and Visbal, 2000 and Beran and Pettit, 2001, which compare well to the current results. A solution point on the trivial branch at $\lambda = 18$ is observed to be lightly stable, bracketing the value of λ at which stability is lost between 18 and 18.5.

At Mach 1.2, a simpler solution structure exists, consistent with the findings of other investigators Gordnier and Visbal, 2000; Dowell, 1967. For this Mach number, the trivial branch of panel solutions is observed to lose stability to a branch of LCO solutions at a value of λ between 17 and 18.5. The Hopf bifurcation is supercritical, and computed data for 4 structural modes are compared to that previously reported in Fig. 2. Agreement is good for prediction of LCO amplitude, LCO onset pressure, and LCO frequency, although here, only comparisons of LCO amplitude and onset are reported. Agreement with the results of Gordnier and Visbal, 2000 are slightly improved with the current procedure over that reported by Beran and Pettit, 2001. LCO amplitude is insensitive to the number of modes used in the structural analysis. For the highly dynamic case corresponding to $\lambda = 100$, $\frac{3}{4}$chord deflections (w_d/h) of 1.5948 ($I_m = 4$), 1.5918 ($I_m = 3$), and 1.6333 ($I_m = 2$) are computed. As solutions for both Mach 0.9 and 1.2 are found to be converged with respect to the number of structural modes when $I_m = 4$, this value is assumed in all results reported below.

3.2. Reduced order analysis

Results obtained with reduced-order representations of the aeroelastic system are now presented for Mach 0.9 and 1.2. First, at Mach 0.9, a ROM is constructed to directly predict the critical value of λ at which the panel loses stability to nontrivial, steady deflections. This procedure is repeated for Mach 1.2 following construction of a second ROM, but in this case, the new ROM is also used in the calculation of LCOs at selected dynamic pressures.

At Mach 0.9, a 10-mode ROM is constructed using 4 steady solutions, computed for $\lambda = 20$ and 30 on the inward- and outward-deflected solution branches. A search procedure, like that described above in the Bifurcation Analysis

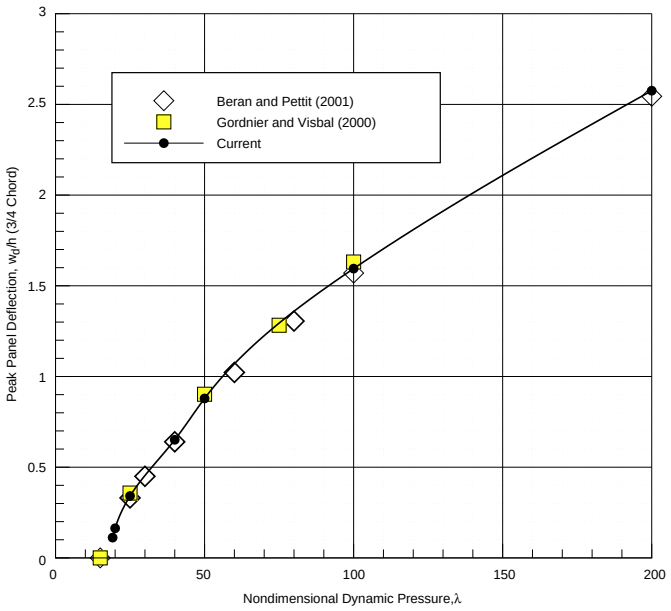

Fig. 2. Comparison of peak dynamic deflections at the panel $\frac{3}{4}$-chord for Mach 1.2 and selected dynamic pressures ($I_m = 4$).

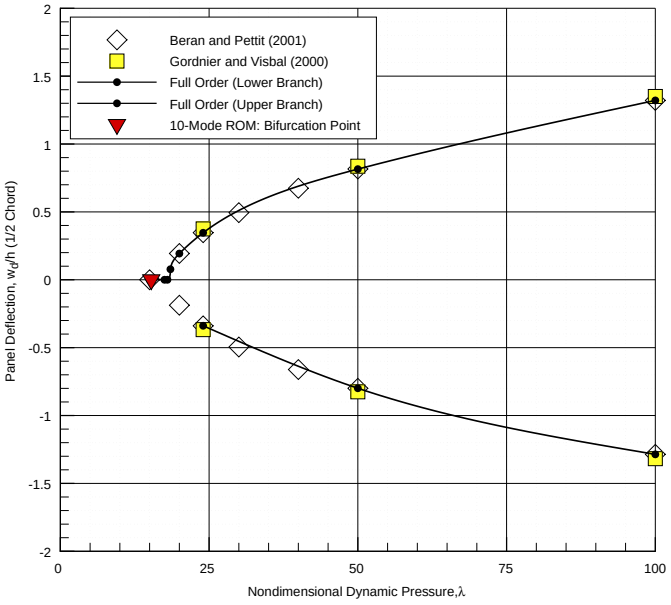

Fig. 3. Bifurcation point directly computed with the ROM method for Mach 0.9 ($\lambda \approx 15.28$) and nontrivial solution branches.

section, is carried out to compute the crossover point ($\beta = 0$). In this case of steady state analysis, attention is restricted to eigenvalues with only real parts. The search procedure is very fast, requiring about 2 CPU minutes on a 1.13 Ghz laptop computer and 10–15 iterations, depending on initial guess and jump size. In comparison, computation of a single steady state solution requires about 2 CPU hours on the same class of computer.

When the 10 most significant modes of the ROM are retained, the location of the bifurcation point is computed to be $\lambda = 15.28$. This value is lower than that found with the full-order analysis, which brackets the bifurcation point between $\lambda = 18$ and 18.5. See Fig. 3. Direct prediction of the bifurcation point, while precise for a specified number of POD modes, is found to be somewhat sensitive to the number of retained modes, M_r. For a moderate number of retained

modes, a trend of decreasing dynamic pressure at the critical point with increasing M_r is established: 17.16 ($M_r = 8$), 16.74 ($M_r = 9$), 15.28 ($M_r = 10$), and 15.05 ($M_r = 11$). When 12 or more modes are retained (up to 16 maximum), the modes appear to lose linear independence, and the results become unreliable. With less than 8 modes, there appears to be too little information representing the system. This last observation is consistent with an expected number of minimum states, which would be the product of the number of physical variables (4) and the number of behaviors to represent (2, i.e., upward and downward deflection of the panel). Thus, for the ROM constructed, the bifurcation point can be considered to lie between about 15 and 17, depending on M_r. Additional attention should be given to the methodology to attempt to reduce this level of uncertainty and to improve the level of agreement with the full-order model.

The reader should note that the current procedure for computing the bifurcation point is about 4 times more efficient than that employed by Beran and Pettit, 2001, owing to the significant reduction in computer time needed to evaluate $\partial\hat{R}/\partial Y_s$ in the modal form of the structure in comparison to the previous finite-difference approach.

Solutions exhibiting accurate LCO behavior are obtained with a POD-based ROM constructed for Mach 1.2 and $\lambda = 25$. This same ROM is used in the direct determination of the critical value of λ at which the panel first loses stability. A 10-mode ROM is constructed from 40 full-system samples, collected at a uniform rate during the first 20 time units of a computation that requires about 300–400 time units to establish LCO. With this number of modes, about 98% of the energy represented by the sampled data is retained. The ROM is found to predict LCO frequency and amplitude with reasonable accuracy up to about $\lambda = 40$. For reasons to be discussed below, a small level of structural damping is assumed in the second mode: $\zeta_2 = 0.01$. The location of the Hopf bifurcation is computed to be at $\lambda = 17.61$, which is consistent with full-order analysis, which brackets the bifurcation point between $\lambda = 17$ and 18.5. At the bifurcation point, the imaginary component of the critical, complex pair is 0.683 radians per time unit, corresponding to a period of 9.20 for the neutral mode. (The reader should note that fully developed LCOs at and below $\lambda = 18.5$ are not computed with full-order analysis owing to the very large computational times necessary to capture these lightly damped solutions.)

LCO solutions are shown in Fig. 4 for ROM solutions computed with $\Delta_t = 0.05$, a time step 10 times larger than that permitted (i.e., by stability) for integration of the full-order system. One subiteration is performed at each step of the time-integration process; additional subiterations have negligible impact on the computed solution. In general, ROM solutions are in excellent agreement with the full-order results for λ less than about 40. In comparison to the ROM solutions presented by Beran and Pettit, 2001, which are not shown in Fig. 4 to maintain figure clarity, the new implicit time-integration methodology allows larger time steps while not degrading accuracy. For the cases examined herein, application of reduced-order modelling is not found to diminish LCO amplitude. The ROM is found to be inaccurate

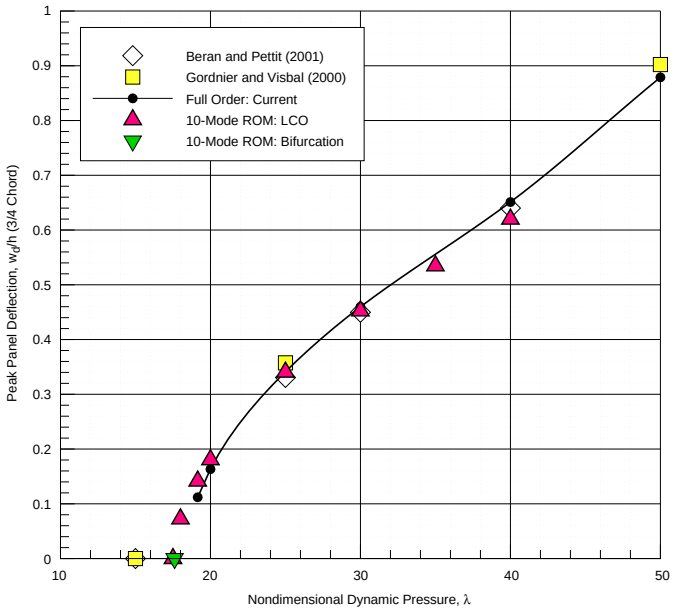

Fig. 4. Comparison of peak deflections at $\frac{3}{4}$-chord location for full-order ($\zeta_2 = 0$) and reduced order ($\zeta_2 = 0.01$) models for Mach 1.2, including ROM-predicted bifurcation point at $\lambda = 17.61$.

when $\Delta_t \geqslant 0.1$. For these large time steps the natural response of the second structural mode does not appear to be properly resolved, thereby permitting the sustainment of a high-frequency error (approximately 10% of the base LCO amplitude).

Time histories of deflections predicted with the 10-mode ROM (constructed for $\lambda = 25$) compare reasonably well with those obtained using full-order analysis. Results are presented in Fig. 5 for a subcritical case, $\lambda = 10$, and in Fig. 6 for a supercritical case, $\lambda = 25$, the value of λ at which the ROM was constructed. In the supercritical case, LCO amplitude and frequency are in excellent agreement, although at large times, there is a slight accumulated phase shift error. When λ is decreased to 10, the aeroelastic system is stable, as predicted by both full-order and reduced order analysis. However, the ROM solution has a lower level of damping than desired.

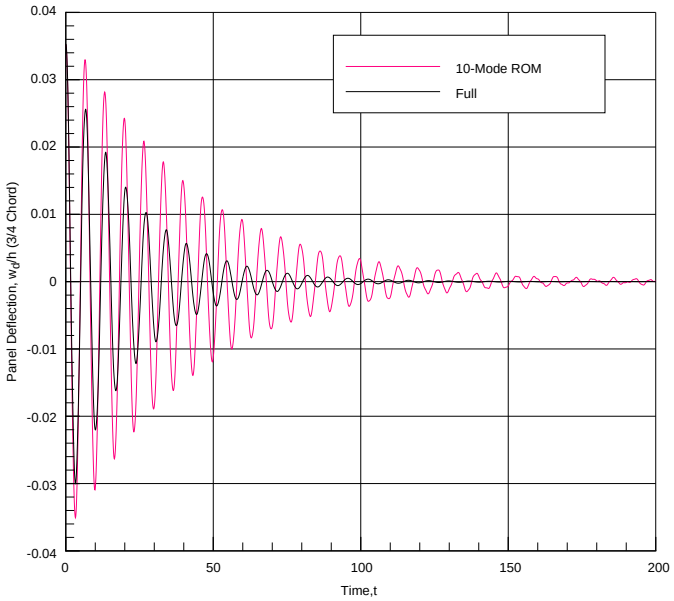

Fig. 5. Comparison of full-order ($\Delta_t = 0.005$) and ROM ($\Delta_t = 0.05$) time histories of $\frac{3}{4}$-chord panel deflection at Mach 1.2 and $\lambda = 10$.

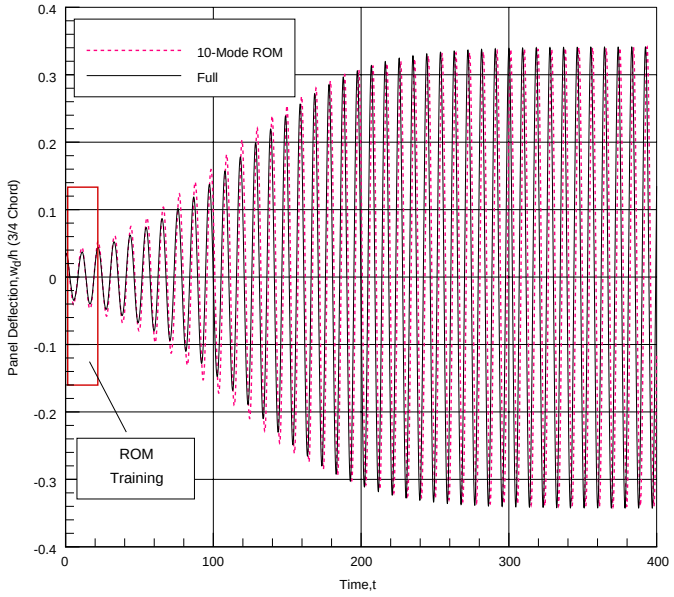

Fig. 6. Comparison of full-order ($\Delta_t = 0.005$) and ROM ($\Delta_t = 0.05$) time histories of $\frac{3}{4}$-chord panel deflection at Mach 1.2 and $\lambda = 25$.

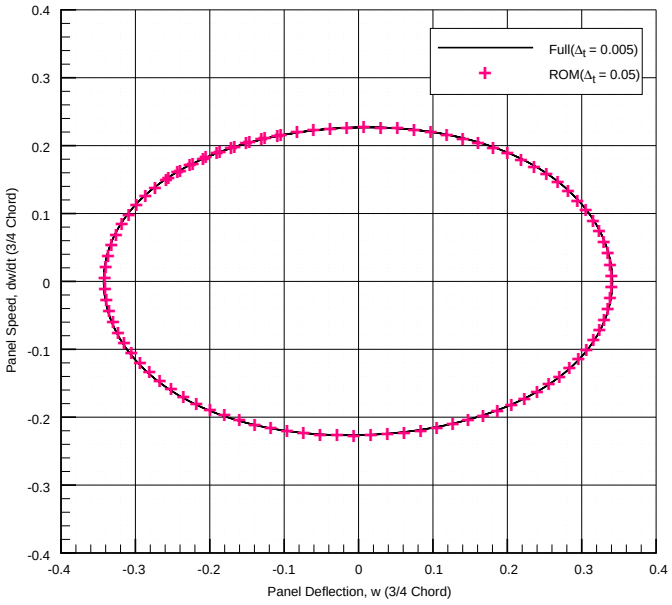

Fig. 7. Comparison of w-dw/dt phase portraits for Mach 1.2 and $\lambda = 25$ ($380 \leqslant t \leqslant 400$).

Full-order and reduced-order solutions are also compared using phase portraits of panel deflection and panel speed (dw/dt) in Fig. 7. In this figure, the fidelity of the ROM with time step of 0.05 (placing about 180 time steps in each cycle) is evident. Sensitivity of the reduced-order solution to time step is confirmed by comparing the peak deflection (3/4 chord) for $\Delta_t = 0.05$ (0.3405) to that of $\Delta_t = 0.025$ (0.3373).

The aeroelastic system is analyzed with much greater computational efficiency using the ROM. The full-order system is analyzed in about 2 CPU hours (a simulation of 400 time units), while the reduced-order system is time-integrated in about one-quarter of the time. The location of the Hopf bifurcation point is predicted even more efficiently, in about 2 CPU minutes. The cost of constructing the ROM is relatively small, approximately one-twentieth that of the complete full-order simulation. Once the ROM is constructed, it can be applied over a fairly wide range of dynamic pressures without change.

The reduced- and full-order models for $\lambda = 25$ are also compared using the amplitudes of the structural modes. As phase portraits during LCO, the computed amplitudes of modes 1 and 2 are compared in Fig. 8, while modes 3 and 4 are shown in Fig. 9. The reader should note that the amplitudes are associated with the deflection as scaled by panel length, and not panel thickness (0.002), leading to the rather small amplitude values reported. The chosen form of presentation highlights differences in modal behaviors; for example, as seen in Fig. 9, the mode 2 response predicted with the ROM is of somewhat greater amplitude. However, the phase relationship between mode 1 and 2 is well preserved, and, since the mode 2 response is small relative to that of mode 1, differences in mode 2 amplitude have little impact on the overall panel response. The amplitudes of modes 3 and 4 are even smaller, possibly weakening their influence during ROM construction, but the general characteristics of the ROM modal responses correspond well to those of the full-order system.

Frequency of LCO response varies in a complicated manner with respect to dynamic pressure, as predicted by the full-order model and the 10-mode ROM trained at $\lambda = 25$. The excellent agreement between the two models is shown in Fig. 10 over a range of values of λ from 10 to 40. Also shown in this figure is the frequency associated with the Hopf bifurcation at $\lambda = 17.61$ predicted by the ROM and an inset figure that magnifies the region of interest around the bifurcation point. Not surprisingly, the reduced order yields an LCO frequency nearly identical to that of the full-order model at $\lambda = 25$. However, the agreement remains good for values of λ at or above 17.5 (within approximately 2%), and a local minimum in frequency near $\lambda = 18.5$ is predicted by both approaches. This figure also shows that the frequency predicted by the direct procedure is reasonably consistent with data obtained with time integration of the ROM. Small differences between time integration and direct analysis of the ROM may be attributable to the large time steps employed and small errors in the computation of frequencies from the time-series data.

The ROM calculations described above are carried out using a small amount of damping in the second mode: $\zeta_2 = 0.01$ (all other damping coefficients set to 0). The purpose of this added damping is to stabilize an unstable,

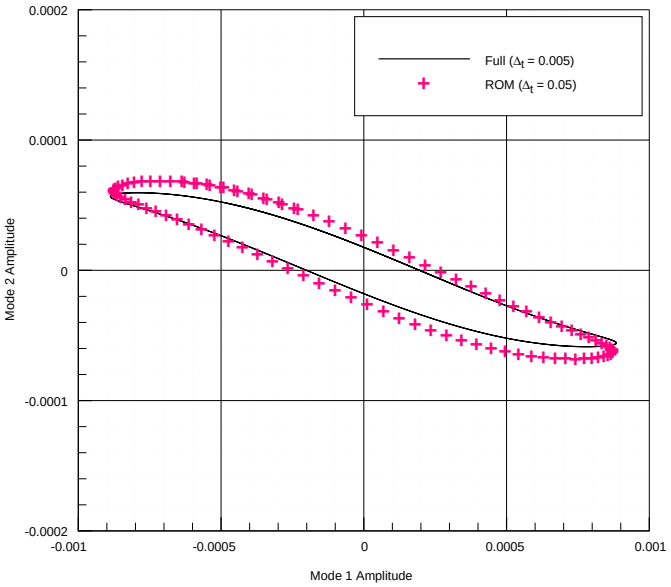

Fig. 8. Comparison of mode $\frac{1}{2}$ amplitudes during LCO ($\lambda = 25$).

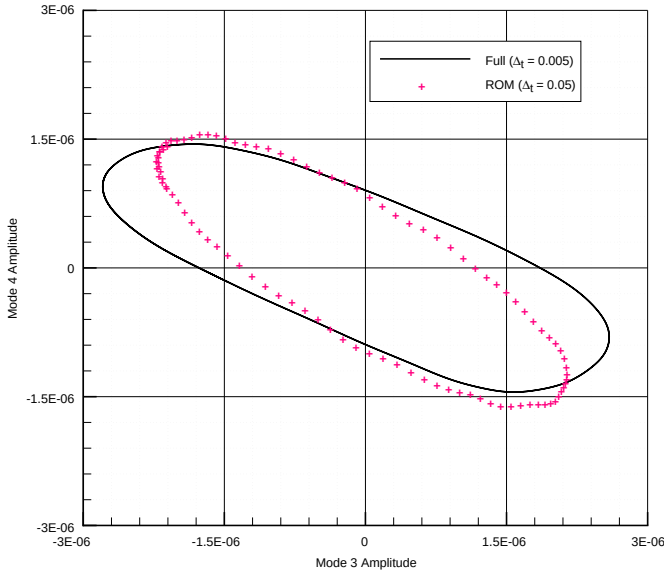

Fig. 9. Comparison of mode $\frac{3}{4}$ amplitudes during LCO ($\lambda = 25$).

complex pair of eigenvalues of the reduced-order aeroelastic system ($\hat{J}$) associated with the second structural mode. The effect of the added damping is demonstrated in Fig. 11, where it is seen that a complex pair in the right-hand plane is moved to the left-hand plane with negligible impact on neighboring eigenvalues. This pair has a frequency of about 3 radians per time unit, which is near the natural frequency of the second mode, 2.50 radians per time unit (the natural frequencies of modes 1, 3, and 4, are 0.624, 5.62, and 9.99 radians per time unit, respectively). Examination of the eigenvector corresponding to the unstable pair also establishes the connection between this pair and the second structural mode. The reader should note that the eigenvalue spectra appearing in Fig. 11 are computed at $\lambda = 17.61$, where the physical bifurcation, primarily involving the first structural mode, occurs.

In contrast, the Hopf bifurcation involving the second structural mode, which the undamped ROM predicts at a value of λ below 17.61, is not physical. Fortunately, the small amount of damping specified removes the undesirable

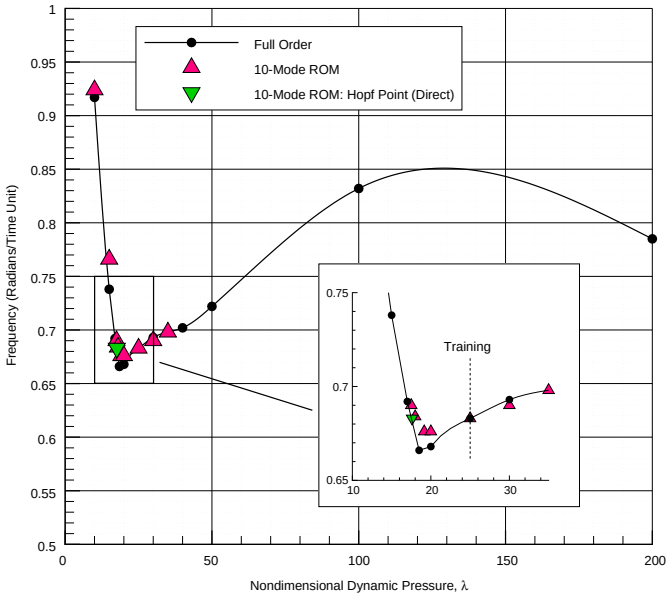

Fig. 10. Comparison of frequencies of oscillation (decaying or growing) for selected dynamic pressures: ROM versus full-order analysis.

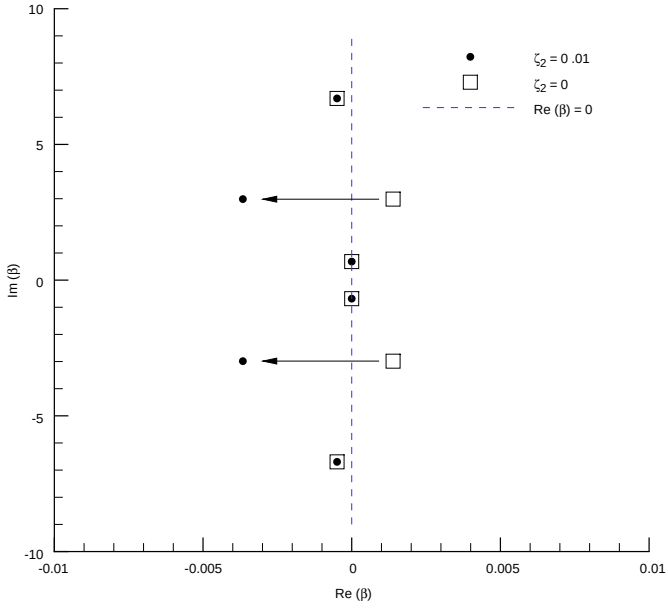

Fig. 11. Truncated eigenvalue spectra of $\hat{J}$ near critical pair for two damping conditions at the bifurcation condition, $\lambda = 17.61$.

behavior, with little effect on the other modes. However, as λ is increased, this troublesome pair again becomes unstable, and by $\lambda = 40$ pollutes the LCO to a degree which cannot be controlled by damping. Such behavior is entirely absent from the response of the full-order model. The authors do not have a complete explanation for how the second structural mode becomes of increased importance in the ROM, but find interesting clues in the data samples used in the construction of the ROM. Time histories of the structural modes are shown in Fig. 12 over the period of time in which data samples are collected. The initial conditions of $a_1(0) = 0.0001$ and $a_i(0) = 0$ $(i \neq 1)$ are found to be satisfied. Upon

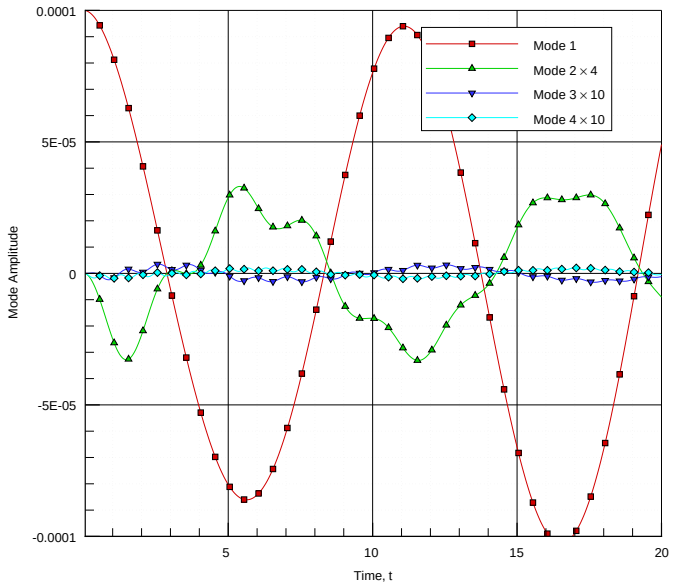

Fig. 12. Time histories of structural modes during ROM construction (response of full-order system at $\lambda = 25$; response of modes 2–4 magnified with only every tenth data point shown by symbol).

release of the panel, modes 2–4 respond in two ways. First, there is are base responses at the response frequency of mode 1. With time, these responses continue to develop until LCO is achieved. Second, there are more rapid responses at about the natural frequencies of the higher modes. In mode 2, the natural response is observed to damp slowly over the training period and to be of relatively large amplitude. We speculate that over the short time interval $0 \leqslant t \leqslant 20$, the perturbations arising from the response of mode 2 in its natural frequency lead to a misidentification of mode 2 behavior in the ROM. Given the results presented above, mode 2 in the ROM appears to be under-damped, perhaps a result of the transient, natural response in mode 2 over-emphasized in the computed POD mode set. The issue of whether this problem can be corrected through an improved training process involving different modal initial conditions, better selection of data snapshots, or judicious application of structural damping, should be addressed in future research.

4. Summary and conclusions

Two aeroelastic models for simulating the interaction between an inviscid flow and a nonlinear panel were developed: a full-order model and a ROM. The full-order model was obtained from a coupling of the discrete Euler equations (fluid) and the discrete von Kármán equation (structure), and contained over 65,000 dof. Solutions of the full-order model for Mach 0.9 and 1.2 provided results that compared well-published results. Full-order solutions were typically computed in about 3 h on a fast workstation.

ROMs were constructed and used according to the following procedure: (1) applying the POD to a collection of full-order data samples; (2) computing a set of POD modes and retaining the dominant modes; (3) projecting the governing fluid equations into the computed subspace and coupling these equations to the structural equations, and (4) time integrating or directly solving the reduced order system. ROMs were obtained for two Mach numbers at which the aerodynamics were reasonably linear: 0.9 and 1.2. At Mach 0.9, available solutions were static, and a 10-mode ROM was constructed from a small set of data samples. Linearization of the ROM and application of a direct search procedure yielded a pitchfork-bifurcation location close to that found through an extensive full-order analysis. The computational cost of this calculation was on the order of minutes, at least two orders of magnitude faster than with the full-order model.

At Mach 1.2, a 10-mode ROM was constructed from a set of full-order data samples computed over a short transient period. This single ROM was then used in LCO simulation for different dynamic pressures and in the computation of the supercritical Hopf bifurcation point at which LCO states became available. LCO states were computed with

reasonable accuracy, in comparison to full-order results, over a range of dynamic pressures encompassing decaying and sustained physical oscillations. Direct computation of the Hopf point was executed in a matter of minutes, again at least two orders of magnitude faster than with the full-order model. It was noteworthy that bifurcation analysis of a reduced-order aeroelastic system constructed away from the critical point accurately predicted bifurcation location and frequency. Also, by increasing the stability-limited time step by an order of magnitude, fully developed LCOs were computed with the ROM 4–5 times faster than with the full-order model. Accuracy of the LCO simulation was maintained for these large time steps by time-synchronizing the fluid and structure through a subiterative procedure. Further research is recommended to determine the sensitivity of the results reported herein to variations in the process by which the ROMs at Mach 0.9 and Mach 1.2 were constructed.

Acknowledgements

The authors gratefully acknowledge the support of the Air Force Office of Scientific Research under grant 99VA01COR (Dr Dean Mook, Program Manager).

References

Beran, P.S., 1998. A domain-decomposition method for airfoil flutter analysis. AIAA Paper 98-0098.

Beran, P.S., 1999. Computation of limit-cycle oscillation using a direct method. AIAA Paper 99-1462.

Cunningham, A.M., 1998. The role of non-linear aerodynamics in fluid-structure interactions, AIAA Paper 98-2423.

Beran, P.S., Morton, S.A., 1997. Continuation method for calculation of transonic airfoil flutter boundaries. Journal of Guidance, Control and Dynamics 20 (6), 1165–1171.

Beran, P.S., Pettit, C.L., 2001. Prediction of nonlinear panel response using proper orthogonal decomposition. AIAA Paper 2001-1292.

Beran, P., Silva, W., 2001. Reduced-order modelling: new approaches for computational physics 39th Aerospace Sciences Meeting, Reno, NV, USA, January 8-11, AIAA paper 2001-0853.

Beran, P.S., Huttsell, L.J., Buxton, B.J., Noll, C., Osswald, G., 1999. Computational aeroelasticity techniques for viscous flow. CEAS/AIAA/ICASE/NASA Langley International Forum on Aeroelasticity and Structural Dynamics, Williamsburg, VA.

Dobbs, S.K., Miller, G.D., Stevenson, J.R., 1985. Self induced oscillation wind tunnel test of a variable sweep wing. Proceedings of the AIAA/ASME/ASCE/AHS 26th Structures, Structural Dynamics and Materials Conference, Orlando, FL, April 15–17, AIAA Paper 85-0739-CP.

Dowell, E.H., 1966. Nonlinear oscillations of a fluttering plate. AIAA Journal 4 (7), 1267–1275.

Dowell, E.H., 1967. Nonlinear oscillations of a fluttering plate. II. AIAA Journal 5, 1856–1862.

Gordnier, R.E., Melville, R.B., 1998. Accuracy issues for transonic wing flutter using 3-D Navier–Stokes. Proceedings of the 39th AIAA/ASME/ASCE/AHS/ASC Structures, Structural Dynamics, and Materials Conference, Long Beach, CA, AIAA Paper 98-1729-CP.

Gordnier, R.E., Visbal, M.R., 2000. Development of a three-dimensional viscous aeroelastic solver for nonlinear panel flutter. AIAA Paper 2000-2337.

Hall, K.C., Thomas, J.P., Dowell, E.H., 2000. Proper orthogonal decomposition technique for transonic unsteady aerodynamic flows. AIAA Journal (also AIAA Paper 99-0655) 38 (10), 1853–1862.

Holmes, P., Lumley, J.L., Berkooz, G., 1996. Turbulence, Coherent Structures, Dynamical Systems and Symmetry. Cambridge University Press, Cambridge.

LeGresley, P.A., Alonso, J.J., 2000. Airfoil design optimization using reduced order models based on proper orthogonal decomposition. AIAA Paper 2000-2545.

LeGresley, P.A., Alonso, J.J., 2001. Investigation of non-linear projection for POD based reduced order models for aerodynamics, AIAA Paper 2001-0926.

Lucia, D.J., Beran, P.S., King, P.K., 2002. Reduced order modelling of an elastic panel in transonic flow. AIAA Paper 2002-1594, (also Journal of Aircraft) 40 (2), 338–347.

Mortara, S.A., Beran, P.S., 2000. A proper orthogonal decomposition technique for the computation of nonlinear panel response. AIAA Paper 2000-1936.

Morton, S.A., Beran, P.S., 1999. Hopf-bifurcation analysis of airfoil flutter at transonic speeds. Journal of Aircraft 36 (2), 421–429.

Newman, A.J., 1996. Model reduction via the Karhunen–Loeve expansion part 1: an exposition. Tech. Rep. T.R. 96-32, Institute for Systems Research, University of Maryland.

Park, H.M., Lee, M.W., 1998. An efficient method of solving the Navier–Stokes equation for flow control. International Journal for Numerical Methods in Engineering 41, 1133–1151.

Pettit, C.L., Beran, P.S., 2000. Reduced-order modeling for flutter prediction. 41st AIAA/ASCE/AHS/ASC Structures, Structural Dynamics and Materials Conference, Atlanta, GA, AIAA Paper 2000-1446-CP; IJNME 55(4) 479–497, to appear.

Rediniotis, O.K., Ko, J., Yue, X., Kurdila, A.J., 1999. Synthetic jets, their reduced order modeling and applications to flow control. 37th Aerospace Sciences Meeting and Exhibit, Reno, N.V., AIAA Paper 99-1000.

Romanowski, M.C., 1996. Reduced order unsteady aerodynamic and aeroelastic models using Karhunen-Loeve eigenmodes. 6th AIAA/USAF/NASA/ISSMO Symposium on Multidisciplinary Analysis and Optimization, Bellevue WA, AIAA 96-3981-CP, pp. 7–13.

Sankar, L.N., Ruo, S.Y., Malone, J.B., 1986. Application of surface transpiration in computational aerodynamics, AIAA 24th Aerospace Sciences Meeting, Reno, NV, AIAA Paper 86-0511.

Selvam, R.P., Morton, S.A., 1998. Computation of nonlinear viscous panel flutter using a fully implicit aeroelastic solver. AIAA Paper 98-1844.

Thomas, J.P., Dowell, E.H., Hall, K.C., 2001. Three-dimensional transonic aeroelasticity using proper orthogonal decomposition based reduced order models. AIAA Paper 2001-1526.